Eur. Phys. J. C (2015) 75:134
DOI 10.1140/epjc/s10052-015-3353-5

THE EUROPEAN PHYSICAL JOURNAL C

Regular Article - Theoretical Physics

Exclusive $b \to s\nu\bar{\nu}$ induced transitions in the RS$_c$ model

P. Biancofiore[1,2,a], **P. Colangelo**[2,b], **F. De Fazio**[2,c], **E. Scrimieri**[1,2,d]

[1] Dipartimento Interateneo di Fisica, Universitá di Bari, via Orabona 4, 70126 Bari, Italy
[2] INFN, Sezione di Bari, via Orabona 4, 70126 Bari, Italy

Received: 10 December 2014 / Accepted: 8 March 2015 / Published online: 24 March 2015

Abstract We study a set of exclusive B and B_s decay modes induced by the rare $b \to s\nu\bar{\nu}$ transition in the RS$_c$ model, an extra-dimensional extension of the standard model with warped 5D metric and extended gauge group. We discuss the role of correlations among the observables, and their importance for detecting the predicted small deviations from the standard model expectations.

1 Introduction

The current searches for deviations from (or for further confirmation of) the Standard Model (SM) involve observables of increasing sophistication and difficulty. This is what happens for several quark flavor observables that are able to provide us with access to large energy scales, complementing the direct searches at the CERN LHC [1–3]. The flavor changing neutral current (FCNC) processes, loop-induced and heavily suppressed in SM, play a prominent role, and an important case to be studied is the $b \to s\nu\bar{\nu}$ transition, which in the SM proceeds through Z^0 penguin and box diagrams dominated by the contribution with the intermediate top quark [4].

Rare b decays with neutrino pairs in the final state are experimentally challenging. Nevertheless, the advent of new high-luminosity B factories opens the possibility to access these modes which, on the other hand, present remarkable features of theoretical clearness, as we discuss below. We are mainly interested in the exclusive $B \to K\nu\bar{\nu}$ and $B \to K^*\nu\bar{\nu}$ decays, the branching fractions of which were predicted in the SM of $\mathcal{O}(10^{-6})$ [5,6]. Since the results are affected by the uncertainty of the form factors parametrizing the hadronic matrix elements, particular attention has to be paid to such an issue. Using form factors from light-cone QCD sum rules together with experimental information on the $B \to K^*\gamma$ decay rate [7], predictions were obtained in the SM [8],

$$\begin{aligned} \mathcal{B}(B^+ \to K^+\nu\bar{\nu}) &= (4.5 \pm 0.7) \times 10^{-6}, \\ \mathcal{B}(B \to K^*\nu\bar{\nu}) &= (6.8^{+1.0}_{-1.1}) \times 10^{-6} \end{aligned} \tag{1}$$

(considering in the final state the sum over the three neutrino species), recently reconsidered on the basis of a combined lattice QCD and light-cone sum rules fit of the form factors [9]. The predictions must be compared to the present experimental upper bounds. The Belle Collaboration has established the limits, at 90 % CL [10],

$$\begin{aligned} \mathcal{B}(B^+ \to K^+\nu\bar{\nu}) &< 5.5 \times 10^{-5}, \\ \mathcal{B}(B^0 \to K^0_S\nu\bar{\nu}) &< 9.7 \times 10^{-5}, \\ \mathcal{B}(B^+ \to K^{*+}\nu\bar{\nu}) &< 4.0 \times 10^{-5}, \\ \mathcal{B}(B^0 \to K^{*0}\nu\bar{\nu}) &< 5.5 \times 10^{-5}. \end{aligned} \tag{2}$$

The bounds (at 90 % CL) obtained by the BaBar Collaboration [11],

$$\begin{aligned} \mathcal{B}(B^+ \to K^+\nu\bar{\nu}) &< 1.6 \times 10^{-5}, \\ \mathcal{B}(B^0 \to K^0\nu\bar{\nu}) &< 4.9 \times 10^{-5}, \\ \mathcal{B}(B^+ \to K^{*+}\nu\bar{\nu}) &< 6.4 \times 10^{-5}, \\ \mathcal{B}(B^0 \to K^{*0}\nu\bar{\nu}) &< 12 \times 10^{-5}, \end{aligned} \tag{3}$$

are derived combining the results of the semileptonic tag reconstruction method [12] and of the hadronic tag reconstruction method [11].

In addition to $B \to K^{(*)}\nu\bar{\nu}$, other modes are induced by the $b \to s\nu\bar{\nu}$ transition, namely $B_s \to (\phi, \eta, \eta', f_0(980))\nu\bar{\nu}$ that we also discuss in the following. At present, the experimental upper bounds for their rates are still quite high [13,14], however, they are also expected to be sizeably reduced at the new high-luminosity B facilities.

The importance of the rare $b \to s\nu\bar{\nu}$ process relies on its particular sensitivity to new interactions. In [15] the effects of scalar and tensor interactions have been discussed, with par-

[a] e-mail: pietro.biancofiore@ba.infn.it
[b] e-mail: pietro.colangelo@ba.infn.it
[c] e-mail: fulvia.defazio@ba.infn.it
[d] e-mail: egidio.scrimieri@ba.infn.it

ticular attention to the distortion of the q^2 spectra (with q^2 the dilepton squared four-momentum) with respect to SM. The role of new right-handed operators has also been discussed [6], and the possibility of non-standard Z couplings to b and s quarks has been considered [16]. An overview of the effects predicted in several new-physics (NP) scenarios is in Ref. [8], and the case of models with partial compositeness has been investigated in [17]. In an analysis of the effects of a new neutral gauge boson Z', the correlations between the branching ratios, as well as between these modes and the decay $B_s \to \mu^+\mu^-$, have been analyzed under different assumptions for the Z' couplings [18]. In extensions of SM based on additional spatial dimensions, predictions have been given for the decay rates and distributions in minimal models with a single universal extra-dimension [19]. Here, we consider the case of a single warped extra-dimension, as formalized in the Randall–Sundrum model [20], in particular in the realization with custodial protection of the $Zb_L\bar{b}_L$ coupling [21–23]. In [24] a range for the $B \to K^{(*)}\nu\bar{\nu}$ branching fractions has been predicted in this framework. Here we extend the analysis focusing on other observables, such as several differential distributions, and on various correlations, reconsidering the predictions using model parameters singled out in a study of the rare semileptonic $B \to K^*\ell^+\ell^-$ modes [25].

In Sect. 2 we describe the general form of the effective $b \to s\nu\bar{\nu}$ Hamiltonian, and in Sect. 3 we define several $B \to K^{(*)}\nu\bar{\nu}$ observables. Generalities of the custodially protected Randall–Sundrum model are described in Sects. 4 and 5, with particular attention to the parameter space bound for the model. The predictions are presented in Sects. 6, 7 and 8, with a discussion of possible improvements. The conclusions are collected in the last section.

2 $b \to s\nu\bar{\nu}$ effective Hamiltonian

In SM the effective $b \to s\nu\bar{\nu}$ Hamiltonian is written as

$$H_{\rm eff}^{\rm SM} = \frac{G_F}{\sqrt{2}}\frac{\alpha}{2\pi\sin^2\theta_W} V_{tb}^* V_{ts} X(x_t)(\bar{b}s)_{V-A}(\bar{\nu}\nu)_{V-A} \equiv C_L^{\rm SM} O_L, \tag{4}$$

with $O_L = (\bar{b}s)_{V-A}(\bar{\nu}\nu)_{V-A}$ [4]. G_F and α are the Fermi and the fine structure constant at the Z^0 scale, respectively, V_{tb} and V_{ts} are elements of the Cabibbo–Kobayashi–Maskawa (CKM) matrix, and θ_W is the Weinberg angle. The contribution of the operator with opposite chirality $O_R = (\bar{b}s)_{V+A}(\bar{\nu}\nu)_{V-A}$ is negligible. The master function X depends on the top quark mass m_t and on the W mass through the ratio $x_t = m_t^2/M_W^2$:

$$X(x_t) = \eta_X X_0(x_t). \tag{5}$$

The function X_0,

$$X_0(x_t) = \frac{x_t}{8}\left[\frac{x_t+2}{x_t-1} + \frac{3x_t-6}{(x_t-1)^2}\log x_t\right], \tag{6}$$

results from the calculation of the loop (penguin and box) diagrams at leading order (LO) in α_s [26], while the factor $\eta_X = 0.994$ accounts for NLO α_s corrections [27]. X is flavor-universal and real, implying that, in the SM, it is possible to relate different modes with a neutrino pair in the final state, namely $B_d \to X_{s,d}\nu\bar{\nu}$ and $K^+ \to \pi^+\nu\bar{\nu}$ or $K^0 \to \pi^0\nu\bar{\nu}$. Such relations continue to hold in NP models with minimal flavor violation.

The presence of a single operator in the Hamiltonian (4) makes the $b \to s\bar{\nu}\nu$ processes easier to study in the SM with respect to other rare decays described by a richer effective Hamiltonian, for instance those induced by the $b \to s\ell^+\ell^-$ transition. Moreover, long-distance effects threatening, e.g., the modes with charged leptons in the final state due to hadron resonance contributions, are absent in modes into neutrino pairs.

In general NP extensions the new operator with opposite chirality O_R can arise and the value of $C_L^{\rm SM}$ can be modified. The effective $b \to s\nu\bar{\nu}$ Hamiltonian is given by

$$H_{\rm eff} = C_L O_L + C_R O_R, \tag{7}$$

with $C_{L,R}$ specific of the NP model. Notice that we only consider massless left-handed neutrinos.

For the inclusive $B \to X_{s,d}\nu\bar{\nu}$ mode, the heavy quark mass expansion allows one to express the decay rate as a sum of terms proportional to inverse powers of the b quark mass. The $\mathcal{O}(\frac{1}{m_b^2})$ corrections are tiny, and the same happens for the q^2 spectrum except for a small portion of the phase-space close to the kinematical end-point [28]. For the exclusive modes, in the SM a source of uncertainty is in the hadronic form factors describing the matrix element of the operator O_L between the B meson and K or K^*. This problem can be circumvented in $K \to \pi\nu\bar{\nu}$ modes, exploiting information on the corresponding semileptonic modes (with one charged final lepton), and invoking isospin symmetry. On the other hand, the uncertainty represented by the renormalization scale in the QCD corrections is reduced by the account of NLO terms through the η_X factor [4]. Another difference with respect to the analogous Kaon decay modes is that in B decays the top quark contribution dominates, while in the Kaon case, namely the charged $K^+ \to \pi^+\nu\bar{\nu}$ decay, also the CKM enhanced intermediate charm contribution has to be considered. This makes the role of the α_s correction more important in the latter channel since $\alpha_s(m_c) > \alpha_s(m_t)$.

In the study of NP effects it is useful to introduce two parameters [6],

$$\varepsilon^2 = \frac{|C_L|^2 + |C_R|^2}{|C_L^{\rm SM}|^2}, \quad \eta = -\frac{{\rm Re}\left(C_L C_R^*\right)}{|C_L|^2 + |C_R|^2}, \tag{8}$$

which probe deviations from SM where $(\varepsilon,\eta)_{\rm SM}=(1,0)$. In particular, η is sensitive to the right-handed operator in the effective Hamiltonian, while ε mainly measures the deviation from SM in the coefficient C_L.

3 $B\to K\nu\bar\nu$ and $B\to K^*\nu\bar\nu$

The analysis of the exclusive $B\to K^{(*)}\nu\bar\nu$ modes requires the hadronic matrix elements. The $B\to K$ matrix element can be parametrized in terms of two form factors,

$$\langle K(p')|\bar s\gamma_\mu b|B(p)\rangle = (p+p')_\mu F_1(q^2)+\frac{m_B^2-m_K^2}{q^2}q_\mu\left(F_0(q^2)-F_1(q^2)\right), \tag{9}$$

with $q=p-p'$ and $F_1(0)=F_0(0)$. Only F_1 is relevant for decays to massless leptons. Two dimensionless quantities can be defined, the normalized neutrino pair invariant mass $s_B=q^2/m_B^2$, and the ratio $\tilde m_K=m_K/m_B$. In SM the decay distribution in s_B reads

$$\frac{{\rm d}\Gamma^{\rm SM}}{{\rm d}s_B}=3\frac{|C_L^{\rm SM}|^2}{96\pi^3}m_B^5\lambda^{3/2}(1,s_B,\tilde m_K^2)|F_1(s_B)|^2, \tag{10}$$

with $C_L^{\rm SM}$ in (4) and $\lambda(x,y,z)$ the triangular function. In the NP case this expression is generalized to

$$\frac{{\rm d}\Gamma}{{\rm d}s_B}=3\frac{|C_L+C_R|^2}{96\pi^3}m_B^5\lambda^{3/2}(1,s_B,\tilde m_K^2)|F_1(s_B)|^2. \tag{11}$$

In both Eqs. (10) and (11) the factor 3 accounts for the sum over the three final neutrino flavors. Modulo a factor of two, the distributions coincide with the distributions in $E_{\rm miss}$, the (missing) energy of the neutrino pair, since $s_B=2x-1+\tilde m_K^2$, with $x=E_{\rm miss}/m_B$, and

$$\frac{{\rm d}\Gamma}{{\rm d}s_B}=\frac{1}{2}\frac{{\rm d}\Gamma}{{\rm d}x}. \tag{12}$$

For the $B\to K^*$ matrix elements, we adopt the usual parametrization in terms of form factors

$$\begin{aligned}\langle K^*(p',\varepsilon)|\bar s\gamma_\mu(1-\gamma_5)b|B(p)\rangle &= \varepsilon_{\mu\nu\alpha\beta}\varepsilon^{*\nu}p^\alpha p'^\beta\frac{2V(q^2)}{m_B+m_{K^*}}\\ &-i\left[\varepsilon_\mu^*(m_B+m_{K^*})A_1(q^2)\right.\\ &-(\varepsilon^*\cdot q)(p+p')_\mu\frac{A_2(q^2)}{m_B+m_{K^*}}-(\varepsilon^*\cdot q)\frac{2m_{K^*}}{q^2}\big(A_3(q^2)\\ &\left.-A_0(q^2)\big)q_\mu\right],\end{aligned} \tag{13}$$

where ε is the K^* polarization vector. The form factors are not all independent; A_3 can be written as

$$A_3(q^2)=\frac{m_B+m_{K^*}}{2m_{K^*}}A_1(q^2)-\frac{m_B-m_{K^*}}{2m_{K^*}}A_2(q^2), \tag{14}$$

and $A_3(0)=A_0(0)$. However, A_3 and A_0 do not play a role in transitions to massless leptons.

Three transversity amplitudes can be defined, which depend either on C_L-C_R or on C_L+C_R:

$$\begin{aligned}\mathscr{A}_0(s_B)&=-\frac{N(s_B)(C_L-C_R)}{\tilde m_{K^*}\sqrt{s_B}}\\ &\times\Big[(1-\tilde m_{K^*}^2-s_B)(1+\tilde m_{K^*})A_1(s_B)\\ &-\lambda(1,\tilde m_{K^*}^2,s_B)\frac{A_2(s_B)}{(1+\tilde m_{K^*})}\Big],\\ \mathscr{A}_\perp(s_B)&=2\sqrt{2}N(s_B)\lambda^{1/2}(1,\tilde m_{K^*}^2,s_B)(C_L+C_R)\frac{V(s_B)}{(1+\tilde m_{K^*})},\\ \mathscr{A}_\parallel(s_B)&=-2\sqrt{2}N(s_B)(C_L-C_R)(1+\tilde m_{K^*})A_1(s_B),\end{aligned} \tag{15}$$

with $\tilde m_{K^*}=m_{K^*}/m_B$ and the function $N(s_B)$ defined as $N(s_B)=\left[\frac{m_B^3 s_B\lambda^{1/2}(1,\tilde m_{K^*}^2,s_B)}{3\cdot2^7\pi^3}\right]^{1/2}$. The differential distributions in s_B for a longitudinally or transversely polarized K^* (with helicity $h=+1$ or $h=-1$) can be written in terms of these amplitudes. Exploiting the definitions (8), one finds for the sum over the three neutrino flavors:

$$\begin{aligned}\frac{{\rm d}\Gamma_L}{{\rm d}s_B}&=3m_B^2\mathscr{A}_0^2=\left(\frac{{\rm d}\Gamma_L}{{\rm d}s_B}\right)_{\rm SM}\varepsilon^2(1+2\eta),\\ \frac{{\rm d}\Gamma_\pm}{{\rm d}s_B}&=\frac{3}{2}m_B^2|\mathscr{A}_\perp\mp\mathscr{A}_\parallel|^2,\\ \frac{{\rm d}\Gamma_T}{{\rm d}s_B}&=\frac{{\rm d}\Gamma_+}{{\rm d}s_B}+\frac{{\rm d}\Gamma_-}{{\rm d}s_B}=3m_B^2\left(\mathscr{A}_\perp^2+\mathscr{A}_\parallel^2\right)\\ &=\left(\frac{{\rm d}\Gamma_T}{{\rm d}s_B}\right)_{\rm SM}\varepsilon^2\left(1+2\eta f_T(s_B)\right),\\ \frac{{\rm d}\Gamma}{{\rm d}s_B}&=3m_B^2\left(\mathscr{A}_0^2+\mathscr{A}_\perp^2+\mathscr{A}_\parallel^2\right)\\ &=\left(\frac{{\rm d}\Gamma}{{\rm d}s_B}\right)_{\rm SM}\varepsilon^2\left(1+2\eta f(s_B)\right),\end{aligned} \tag{16}$$

with

$$\begin{aligned}f_T(s_B)&=\frac{(1+\tilde m_{K^*})^4[A_1(s_B)]^2-\lambda[V(s_B)]^2}{(1+\tilde m_{K^*})^4[A_1(s_B)]^2+\lambda[V(s_B)]^2},\\ f(s_B)&=\frac{\mathscr{F}_1+\mathscr{F}_2}{\mathscr{F}_1+\mathscr{F}_3},\end{aligned} \tag{17}$$

given in terms of

$$\begin{aligned}\mathscr{F}_1&=\left[(1+\tilde m_{K^*})^2(1-s_B-\tilde m_{K^*}^2)A_1(s_B)-\lambda A_2(s_B)\right]^2,\\ \mathscr{F}_2&=8\tilde m_{K^*}^2 s_B\left[(1+\tilde m_{K^*})^4[A_1(s_B)]^2-\lambda[V(s_B)]^2\right],\\ \mathscr{F}_3&=8\tilde m_{K^*}^2 s_B\left[(1+\tilde m_{K^*})^4[A_1(s_B)]^2+\lambda[V(s_B)]^2\right].\end{aligned} \tag{18}$$

In Eqs. (17) and (18) we use the notation $\lambda=\lambda(1,\tilde m_{K^*}^2,s_B)$; the factor 3 in Eq. (16) accounts for the sum over the neutrino species. Also in this case, the distributions in s_B can be converted in neutrino missing energy distributions using Eq. (12).

Starting from the above defined quantities, several observables can be constructed.

The polarization fractions $F_{L,T}$ can be considered [8],

$$\frac{\mathrm{d}F_{L,T}}{\mathrm{d}s_B} = \frac{\mathrm{d}\Gamma_{L,T}/\mathrm{d}s_B}{\mathrm{d}\Gamma/\mathrm{d}s_B} \tag{19}$$

in which several hadronic and parametric uncertainties are reduced or even canceled (namely the overall quantities, like the CKM elements in the SM). The integrated polarization fractions can be obtained, integrating separately the numerator and the denominator in Eq. (19):

$$F_{L,T} = \frac{1}{\Gamma}\int_0^{1-\tilde{m}^2_{K^*}} \mathrm{d}s_B \frac{\mathrm{d}F_{L,T}}{\mathrm{d}s_B}. \tag{20}$$

Another observable is the ratio of branching fractions involving K and the transversely polarized K^* [6],

$$R_{K/K^*} = \frac{\mathscr{B}(B \to K \nu\bar{\nu})}{\mathscr{B}(B \to K^*_{h=-1}\nu\bar{\nu}) + \mathscr{B}(B \to K^*_{h=+1}\nu\bar{\nu})}, \tag{21}$$

which is sensitive to η.

In [6] the transverse asymmetry has been proposed

$$A_T = \frac{\mathscr{B}(B \to K^*_{h=-1}\nu\bar{\nu}) - \mathscr{B}(B \to K^*_{h=+1}\nu\bar{\nu})}{\mathscr{B}(B \to K^*_{h=-1}\nu\bar{\nu}) + \mathscr{B}(B \to K^*_{h=+1}\nu\bar{\nu})}, \tag{22}$$

for which a reduced hadronic uncertainty is expected. However, its measurement would require the determination of the lepton pair polarization [29], therefore we consider it only for a theoretical analysis.

The observables can probe NP effects, as the ones envisaged in warped five-dimensional extensions of the standard model.

4 Randall–Sundrum model with custodial protection

The motivation of the Randall–Sundrum (RS) model is the possibility of addressing, among others, the hierarchy and the flavor problems invoking the same geometrical mechanism [20]. For a description of the model, in particular for the flavor phenomenology, we refer to [30]. Here we briefly illustrate the main features of the custodially protected RS$_c$ model, adopting the same notations of our analysis of $B \to K^*\ell^+\ell^-$ in this framework [25], with the parameter space determined there.

The RS$_c$ model is a new physics scenario in which the spacetime is supposed to be five-dimensional with coordinates (x, y), x being the ordinary 4D Minkowskian coordinates, and metric

$$\mathrm{d}s^2 = e^{-2ky}\eta_{\mu\nu}\mathrm{d}x^\mu \mathrm{d}x^\nu - \mathrm{d}y^2,$$
$$\eta_{\mu\nu} = \mathrm{diag}(+1, -1, -1, -1). \tag{23}$$

The (fifth) coordinate y varies in the range $0 \le y \le L$; $y = 0$ is identified with the so-called UV brane, $y = L$ with the IR brane. To address the hierarchy problem, the parameter k in the metric (23) is chosen $k \simeq \mathscr{O}(M_{\mathrm{Planck}})$: specifically, k is set to $k = 10^{19}$ GeV. We adopt the variant of the model based on the gauge group

$$SU(3)_c \times SU(2)_L \times SU(2)_R \times U(1)_X \times P_{L,R}, \tag{24}$$

which, together with the metric, defines the Randall–Sundrum model with custodial protection RS$_c$ [21–23]. Indeed, the action of the discrete Z_2 $P_{L,R}$ symmetry, implying a mirror action of the two $SU(2)_{L,R}$ groups, guarantees the custodial protection avoiding large Z couplings to left-handed fermions, experimentally not allowed.

Appropriate boundary conditions (BC) on the UV brane permit to break the gauge group (24) to the SM gauge group, which further undergoes a spontaneous symmetry breaking through a Higgs mechanism, as in the SM. Among the various SM fields, the Higgs one is chosen to be localized close to the IR brane, while all the other fields can propagate in the bulk. Here we consider a Higgs field completely localized at $y = L$.

The existence of a compact fifth dimension leads to a tower of Kaluza–Klein (KK) excitations for all particles. As customary in extra-dimensional models, particles having a SM correspondent can be distinguished from those without SM partners by the choice of their field boundary conditions, so that only for some choices a zero-mode in the KK mode expansion exists. Two choices for BC are adopted: Neumann BC on both branes (++), or Dirichlet BC on the UV brane and Neumann BC on the IR one (−+). The zero-modes exist only for fields with (++) BC and are identified with the SM particles. The KK decomposition has the general form

$$F(x, y) = \frac{1}{\sqrt{L}}\sum_k F^{(k)}(x) f^{(k)}(y). \tag{25}$$

For each field $F(x, y)$ the functions $f^{(k)}(y)$ are referred to as the 5D field profiles, and $F^{(k)}(x)$ are the effective 4D fields. The 5D profiles are obtained from the 5D Lagrangian densities for the various fields, solving the resulting 5D equations of motion. This can be performed before the EWSB takes place [30]. Afterwards, the ratio v/M_{KK} of the Higgs vacuum expectation value (vev) v and the mass of the lowest KK mode M_{KK} is treated as a perturbation. The effective 4D Lagrangian is derived integrating over y, and the Feynman rules follow after the neglect of terms of $\mathscr{O}(v^2/M^2_{KK})$, or higher. The mixing occurring between SM fermions and higher KK fermion modes is neglected, being $\mathscr{O}(v^2/M^2_{KK})$. In the case of gauge bosons, modes up to the first KK excitation (1-mode) are taken into account [30].

Among the particles without a SM counterpart, new gauge bosons are predicted to exist, due to the enlarged gauge group.

The gauge bosons of $SU(2)_L$ and $SU(2)_R$ are denoted by $W_L^{a,\mu}$ and $W_R^{a,\mu}$ $(a = 1, 2, 3)$, respectively; the gauge choices $W_{L,R}^{a,5} = 0$ and $\partial_\mu W_{L,R}^{a,\mu} = 0$ are adopted, as for all the other gauge bosons. The equality $g_L = g_R = g$ for the $SU(2)_{L,R}$ gauge couplings is a consequence of the $P_{L,R}$ symmetry.

The eight gauge fields corresponding to $SU(3)_c$ remain identified with the gluons as in the SM, while a new gauge field X_μ, from the $U(1)_X$, has coupling g_X. All the 5D couplings are dimensionful, and are connected to their 4D counterparts by the relation $g^{4D} = g^{5D}/\sqrt{L}$.

A mixing occurs among the various gauge fields. Charged gauge bosons are defined as in the SM:

$$W^{\pm}_{L(R)\mu} = \frac{W^1_{L(R)\mu} \mp i W^2_{L(R)\mu}}{\sqrt{2}}. \tag{26}$$

On the other hand, W_R^3 and X mix through an angle ϕ. The resulting fields are Z_X and B; the latter mixes with W_L^3 with an angle ψ, providing the Z and A fields as in SM.

In summary, the gauge boson content of the model, together with the BC, is: eight gluons G_μ with BC $(++)$, four charged bosons $W_L^{\pm}(++)$ and $W_R^{\pm}(-+)$, three neutral bosons $A(++)$, $Z(++)$, and $Z_X(-+)$. For each of these vector fields, the KK expansion is

$$V_\mu(x, y) = \frac{1}{\sqrt{L}} \sum_{n=0}^{\infty} V_\mu^{(n)}(x) f_V^{(n)}(y). \tag{27}$$

The profiles of the zero-modes are flat, $f_V^{(0)}(y) = 1$. As for the 1-modes, for gauge bosons having a zero-mode they are denoted by $g(y)$ and their mass is denoted M_{++}; for gauge bosons without a zero-mode, they are indicated by $\tilde{g}(y)$, with mass M_{-+}. We refer to the Appendix of [25] for the expressions of these quantities and for the notation. The solution of the equation of motion provides $M_{++} \simeq 2.45 f$ and $M_{-+} \simeq 2.40 f$, where f is the dimensionful parameter $f = k e^{-kL}$. We set this parameter to $f = 1$ TeV, coherently with other studies [31–33].

Before the EWSB the zero-modes of the gauge bosons (if present) are massless, while higher KK excitations are massive. Since the two groups $SU(3)$ (for QCD) and $U(1)_{em}$ remain unbroken, the zero-modes of gluons and photon are massless as in the SM, but their KK excitations are massive.

Mixing also occurs among zero-modes and higher KK modes of gauge fields. Neglecting modes with KK number larger than 1, the mixing involves the charged bosons $W_L^{\pm(0)}$, $W_L^{\pm(1)}$ and $W_R^{\pm(1)}$, with the result

$$\begin{pmatrix} W^{\pm} \\ W_H^{\pm} \\ W'^{\pm} \end{pmatrix} = \mathscr{G}_W \begin{pmatrix} W_L^{\pm(0)} \\ W_L^{\pm(1)} \\ W_R^{\pm(1)} \end{pmatrix}, \tag{28}$$

and the neutral bosons $Z^{(0)}$, $Z^{(1)}$, and $Z_X^{(1)}$ according to the pattern:

$$\begin{pmatrix} Z \\ Z_H \\ Z' \end{pmatrix} = \mathscr{G}_Z \begin{pmatrix} Z^{(0)} \\ Z^{(1)} \\ Z_X^{(1)} \end{pmatrix}. \tag{29}$$

The expressions of the matrices $\mathscr{G}_W$ and $\mathscr{G}_Z$, and the masses of the mass eigenstates can be found in Ref. [30].

Moving to the Higgs sector, the Higgs field $H(x, y)$ transforms as a bidoublet under $SU(2)_L \times SU(2)_R$ and as a singlet under $U(1)_X$. It contains two charged and two neutral components:

$$H(x, y) = \begin{pmatrix} \frac{\pi^+}{\sqrt{2}} & -\frac{h^0 - i\pi^0}{2} \\ \frac{h^0 + i\pi^0}{2} & \frac{\pi^-}{\sqrt{2}} \end{pmatrix}.$$

Its KK decomposition reads

$$H(x, y) = \frac{1}{\sqrt{L}} \sum_k H^{(k)}(x) h^{(k)}(y). \tag{30}$$

The localization on the IR brane leads to the profile

$$h(y) \equiv h^{(0)}(y) \simeq e^{kL} \delta(y - L). \tag{31}$$

Furthermore, one chooses that only the neutral field h^0 has a non-vanishing vacuum expectation value $v = 246.22$ GeV, as in the SM.

The most involved sector is the fermion one. We refer to [30] for the description of the fermion representations. Here, we mention that, considering three generations of quarks and leptons, SM left-handed doublets are collected in a bidoublet of $SU(2)_L \times SU(2)_R$, together with two new fermions. Right-handed up-type quarks are singlets, while no corresponding fields exist in the case of leptons, for left-handed neutrinos. Right-handed down-type quarks, as well as charged leptons are in multiplets transforming as $(3, 1) \oplus (1, 3)$ under $SU(2)_L \times SU(2)_R$, and additional new fermions are also present in such multiplets. The electric charge is related to the third component of the $SU(2)_L$ and $SU(2)_R$ isospins and to the charge Q_X through the equation $Q = T_L^3 + T_R^3 + Q_X$.

The presence of new fermions will not affect our analysis, since we only take into account the zero-modes of SM quarks and leptons. The zero-mode profiles are obtained solving the equations of motion for ordinary fermions, with the result denoted $f_{L,R}^{(0)}(y, c)$:

$$f^{(0)}(y, c) = \sqrt{\frac{(1 - 2c)kL}{e^{(1-2c)kL} - 1}} e^{-cky}. \tag{32}$$

The difference between right- and left-handed fermion profiles lies in the parameter c, the fermion mass in the bulk. Fields belonging to the same $SU(2)_L \times SU(2)_R$ multiplet share the same value of c, as is the case for u_L and d_L, c_L and s_L, t_L, and b_L, as well as for ν_ℓ and ℓ_L^- $(\ell = e, \mu, \tau)$. We choose real c parameters.

Other parameters of the model enter when considering the quark mixing. As in the SM, quark mass eigenstates are obtained by a rotation of flavor eigenstates. The rotation matrices of up-type left (right) and down-type left (right) quarks are denoted by $\mathscr{U}_{L(R)}$, $\mathscr{D}_{L(R)}$, respectively. Moreover, the CKM matrix is obtained as $V_{\rm CKM} = \mathscr{U}_L^\dagger \mathscr{D}_L$. At odds with SM, in which the presence of the CKM matrix affects only charged current interactions, in RS$_c$ the rotation matrices also affect neutral current interactions, and this leads to the occurrence of flavor changing neutral currents at tree level mediated by the three neutral EW gauge bosons Z, Z', Z_H, as well as by the first KK mode of the photon and of the gluon (however, gluons play no role in processes with leptons in the final state, and photons do not contribute to the transitions to neutrinos). The corresponding Feynman rules involve the overlap integrals of fermion and gauge boson profiles,

$$\begin{aligned}\mathscr{R}_{f_i f_j} &= \frac{1}{L}\int_0^L \mathrm{d}y e^{ky} f^{(0)}_{f_i}(y,c_i) f^{(0)}_{f_j}(y,c_j) g(y),\\ \tilde{\mathscr{R}}_{f_i f_j} &= \frac{1}{L}\int_0^L \mathrm{d}y e^{ky} f^{(0)}_{f_i}(y,c_i) f^{(0)}_{f_j}(y,c_j) \tilde{g}(y),\end{aligned} \tag{33}$$

collected in two matrices $\mathscr{R}_f = \mathrm{diag}\left(\mathscr{R}_{f_1 f_1}, \mathscr{R}_{f_2 f_2}, \mathscr{R}_{f_3 f_3}\right)$ and $\tilde{\mathscr{R}}_f = \mathrm{diag}\left(\tilde{\mathscr{R}}_{f_1 f_1}, \tilde{\mathscr{R}}_{f_2 f_2}, \tilde{\mathscr{R}}_{f_3 f_3}\right)$. After the rotation to mass eigenstates, the quantities appearing in the Feynman rules of the model are the products $\mathscr{M}^\dagger \mathscr{R}_f \mathscr{M}$, where $\mathscr{M} = \mathscr{U}_{L,R}, \mathscr{D}_{L,R}$. The details as well as the list of Feynman rules can be found in [25,30].

The required elements of the rotation matrices can be written in terms of the quark profiles, and of the 5D Yukawa couplings denoted by λ^u_{ij} for up-type quarks and λ^d_{ij} for down-type quarks, respectively. The effective 4D Yukawa couplings are given by

$$Y^{u(d)}_{ij} = \frac{1}{\sqrt{2}}\frac{1}{L^{3/2}}\int_0^L \mathrm{d}y \lambda^{u(d)}_{ij} f^{(0)}_{q^i_L}(y) f^{(0)}_{u^j_R(d^j_R)}(y) h(y). \tag{34}$$

This relation produces the fermion mass and mixing hierarchy, due to the exponential dependence of the fermion profiles on the bulk mass parameters [34,35].

The elements of the matrices $\mathscr{U}_{L(R)}$ and $\mathscr{D}_{L(R)}$ are not all independent, not only because the constraint $V_{\rm CKM} = \mathscr{U}_L^\dagger \mathscr{D}_L$ must be fulfilled, but also because the Yukawa couplings determine the quark masses. In particular, the following relations must be satisfied:

$$\begin{aligned} m_u &= \frac{v}{\sqrt{2}}\frac{\det(\lambda^u)}{\lambda^u_{33}\lambda^u_{22} - \lambda^u_{23}\lambda^u_{32}}\frac{e^{kL}}{L} f_{u_L} f_{u_R},\\ m_c &= \frac{v}{\sqrt{2}}\frac{\lambda^u_{33}\lambda^u_{22} - \lambda^u_{23}\lambda^u_{32}}{\lambda^u_{33}}\frac{e^{kL}}{L} f_{c_L} f_{c_R},\\ m_t &= \frac{v}{\sqrt{2}}\lambda^u_{33}\frac{e^{kL}}{L} f_{t_L} f_{t_R}, \end{aligned} \tag{35}$$

as well as the analogous relations for down-type quarks with the replacement $\lambda^u \to \lambda^d$ (with the notation $f_{q_{L,R}} = f^{(0)}_{q_{L,R}}(y = L, c_{q_{L,R}})$). We use the relations (35) to get rid of $\lambda^{u,d}_{11}$, $\lambda^{u,d}_{22}$, $\lambda^{u,d}_{33}$, and express them in terms of the quark masses and of the bulk mass parameters that enter in the profile functions f_{q_L}, f_{q_R}. These are approximate relations, and in principle an uncertainty in the quark masses should be taken into account in order to use them as safely as possible. We have checked that, among the quark masses, the one that has the highest impact, as far as the present calculation is concerned, is the b quark mass. Hence, we choose to treat differently the b quark bulk mass parameter with respect to those of the other quarks. In the next section we describe in detail the strategy for the numerical analysis.

We also adopt simplifying assumptions discussed in [25], such as considering real and symmetric matrices $\lambda^{u,d}$, since in CP-averaged observables the constraints on the phases in new-physics amplitudes are less important than for the absolute values.[1] After the quark mass constraints have been imposed, there are six independent entries among the elements of the $\lambda^{u,d}$ matrices, which we choose [25]

$$\begin{aligned} &\lambda^u_{12}, \quad \lambda^u_{13}, \quad \lambda^u_{23},\\ &\lambda^d_{12}, \quad \lambda^d_{13}, \quad \lambda^d_{23}. \end{aligned} \tag{36}$$

The set of input parameters in our analysis is restricted to the quantities in (36) together with the bulk mass parameters. Before describing our strategy for the numerical study, we discuss the Wilson coefficients in the effective Hamiltonian (7) in RS$_c$, and how they are modified with respect to the standard model.

5 Effective $b \to s\nu\bar{\nu}$ Hamiltonian in RS$_c$ model

In SM the Wilson coefficients of the left- and right-handed operators O_L and O_R in the effective Hamiltonian (4), (7) are given by

$$\begin{aligned} C_L^{\rm SM} &= \frac{G_F}{\sqrt{2}}\frac{\alpha}{2\pi \sin^2\theta_W} V^*_{tb} V_{ts} X(x_t),\\ C_R^{\rm SM} &= 0. \end{aligned} \tag{37}$$

These coefficients are modified in the RS$_c$, in which a right-handed operator O_R is present:

$$C_L^{\rm RS} = \frac{G_F}{\sqrt{2}}\frac{\alpha}{2\pi \sin^2\theta_W} V^*_{tb} V_{ts} X_L^{\rm RS}, \tag{38}$$

$$C_R^{\rm RS} = \frac{G_F}{\sqrt{2}}\frac{\alpha}{2\pi \sin^2\theta_W} V^*_{tb} V_{ts} X_R^{\rm RS}, \tag{39}$$

[1] A general parametrization of the matrices $\lambda^{u,d}$ is described in [31].

with $X_L^{\rm RS} = X(x_t) + \Delta X_L$ and

$$\Delta X_L = \frac{1}{V_{tb}V_{ts}^*} \sum_{X=Z,Z',Z_H} \frac{\Delta_L^{bs}(X)\Delta^{\nu\bar{\nu}}(X)}{4M_X^2 g_{\rm SM}^2}, \tag{40}$$

$$X_R^{\rm RS} = \frac{1}{V_{tb}V_{ts}^*} \sum_{X=Z,Z',Z_H} \frac{\Delta_R^{bs}(X)\Delta^{\nu\bar{\nu}}(X)}{4M_X^2 g_{\rm SM}^2}. \tag{41}$$

The constant $g_{\rm SM}^2$ is defined as $g_{\rm SM}^2 = \dfrac{G_F}{\sqrt{2}} \dfrac{\alpha}{2\pi \sin^2(\theta_W)}$. $\Delta_{L,R}^{f_i f_j}(X)$ is the coupling of a gauge boson X to a pair of fermions $f_i f_j$; it can be read from the Feynman rules described in the appendix of Ref. [25].

The new contributions can be evaluated scanning the parameter space of the RS$_c$ model. As described in [25], we require that the elements of the matrices $\lambda^{u,d}$ lie in a range assuring the perturbativity of the model up to the scale of the first three KK modes: $|\lambda_{ij}^{d,u}| \leq 3/k$. Moreover, the diagonal elements of such matrices are fixed imposing the quark mass constraints. The six remaining parameters, those in (36), must be fixed together with the bulk mass parameters for the quarks, enforcing quark mass and CKM constraints. Imposing for the quark masses the values obtained at the scale $\mathcal{O}(M_{KK})$ through renormalization group evolution, starting from

$$m_d = 4.9\ {\rm MeV}, \quad m_s = 90\ {\rm MeV}, \quad m_b = 4.8\ {\rm GeV}, \tag{42}$$

the following quark mass bulk parameters have been determined [36]:

$$\begin{aligned} &c_L^{u,d} = 0.63, \quad c_L^{c,s} = 0.57, \quad c_L^{b,t} \in [0.40, 0.45], \\ &c_R^{u} = 0.67, \quad c_R^{c} = 0.53, \quad c_R^{t} = -0.35, \\ &c_R^{d} = 0.66, \quad c_R^{s} = 0.60, \quad c_R^{b} = 0.57. \end{aligned} \tag{43}$$

We consider a range in the case of the left-handed doublet of the third quark generation, which is compatible with the constraints derived in [37,38] using the measurements of the coupling $Z\bar{b}b$, of the b-quark left-right asymmetry parameter and of the forward-backward asymmetry for b quarks [39]. Among the mass parameters, this is the one with major impact on the final results.

For leptons, the bulk masses are set to $c_\ell = 0.7$ [24]. Other numerical determinations of the fermion bulk mass parameters can be found in [37,38,40–47].

In correspondence to the values fixed above, we generate the six λ parameters in Eq. (36) imposing the CKM constraints. Specifically, we require $|V_{cb}|$ and $|V_{ub}|$ in the largest range found from their experimental determinations from inclusive and exclusive B decays [14], and that $|V_{us}|$ lies within 2 % of the central value reported by the Particle Data Group [13]. Hence, the selected ranges are:

$$\begin{aligned} &|V_{cb}| \in [0.038 - 0.043], \\ &|V_{ub}| \in [0.00294 - 0.00434], \\ &|V_{us}| \in [0.22 - 0.23]. \end{aligned} \tag{44}$$

The parameter space is further restricted, as in [25], imposing the requirement that the $B \to K^*\mu^+\mu^-$ and $B \to X_s\gamma$ branching fractions lie within the 2σ range of the measurements

$$\mathscr{B}(B \to K^*\mu^+\mu^-)_{\rm exp} = (1.02 \pm^{0.14}_{0.13} \pm 0.05) \times 10^{-6}, \tag{45}$$

$$\mathscr{B}(B \to X_s\gamma)_{\rm exp} = (3.43 \pm 0.21 \pm 0.07) \times 10^{-4}. \tag{46}$$

The datum (45) is the BaBar average of the branching fractions of the four modes $B^{+,0} \to K^{*+,0}\mu^+\mu^-$ and $B^{+,0} \to K^{*+,0}e^+e^-$ [48], while the value in (46) is the HFAG Collaboration average for this inclusive rare radiative B decay width [14]. With the selected set of points in the parameter space it is also possible to reproduce in the RS$_c$ model, using the expressions in [31], the mass difference of the neutral B_s mesons ΔM_s within 20 % of the central value of the experimental measurement $\Delta M_s = 17.69\ {\rm ps}^{-1}$ [14].

Scanning the parameter space resulting from all the constraints, we obtain the coefficients $C_L^{\rm RS}$ and $C_R^{\rm RS}$ and their correlation, as shown in Fig. 1. The resulting parameters η and ε, defined in (8), are depicted in Fig. 2. The first observation concerns the right-handed coupling: we find that a deviation from SM is predicted, with the maximum value $C_R^{\rm RS} = 0.186 \times 10^{-9}\ {\rm GeV}^{-2}$. For the left-handed coupling we obtain the maximum $\Delta C_L = C_L^{\rm RS} - C_L^{\rm SM} = -0.011 \times 10^{-9}\ {\rm GeV}^{-2}$. The largest deviation of η from its SM value $\eta = 0$ is $\eta = -0.075$. We find that C_L and C_R are anticorrelated, as shown Fig. 1, and this has a definite impact on the various observables that we are going to discuss in detail. A reason for such a behavior can be traced to the quite large value reachable for C_R, a point which we comment below.

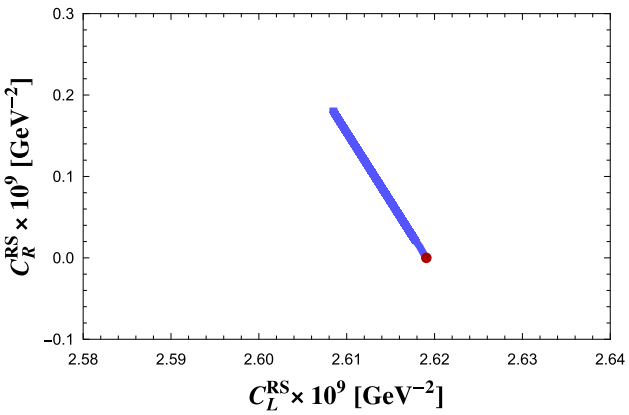

Fig. 1 Correlation between $C_R^{\rm RS}$ and $C_L^{\rm RS}$ in the RS$_c$ model (*blue curve*). *The red dot* corresponds to the central SM values

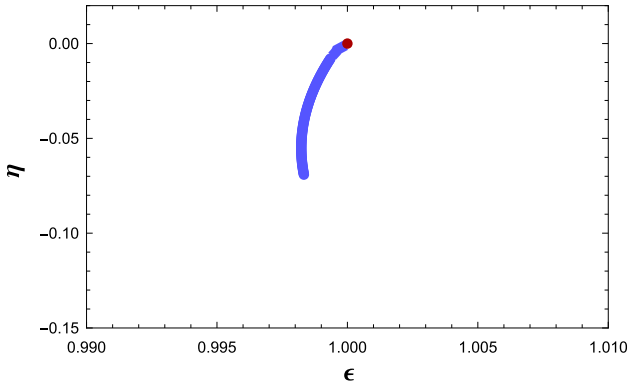

Fig. 2 Correlation between the parameters η and ε, defined in (8), in the RS$_c$ model (*blue curve*). *The red dot* corresponds to the SM

6 $B \to K\nu\bar{\nu}$ and $B \to K^*\nu\bar{\nu}$ observables in RS$_c$

To compare the RS$_c$ predictions to the SM results for the exclusive $B \to K\nu\bar{\nu}$ and $B \to K^*\nu\bar{\nu}$ decay observables defined in Sect. 3 we need the $B \to K^{(*)}$ form factors. Here we use the light-cone QCD sum rule determination [49,50]. Other QCD sum rule determinations, as the one in [51] from three-point correlation functions, have larger uncertainties. The one in [7], which includes QCD factorization corrections, only provides the $B \to K^*$ matrix elements, while we need the full set of $B \to K$, $B \to K^*$, as well as $B_s \to \phi$ matrix elements. Lattice QCD results are now available [52,53], and we comment below on the differences.

In Fig. 3 we depict the differential distribution $\frac{\mathrm{d}\mathscr{B}}{\mathrm{d}s_B}(B^0 \to K^0\nu\bar{\nu})$ in the whole kinematical range $0 \le s_B \le \left(1 - \frac{m_K}{m_B}\right)^2$ in the SM, including the uncertainty on the form factor $F_1(0)$ quoted in [49,50] and using the measured lifetime $\tau(B^0) = 1.519 \pm 0.005$ ps [14]. The predicted branching fraction

$$\mathscr{B}(B^0 \to K^0\nu\bar{\nu})_{\mathrm{SM}} = (4.6 \pm 1.1) \times 10^{-6} \tag{47}$$

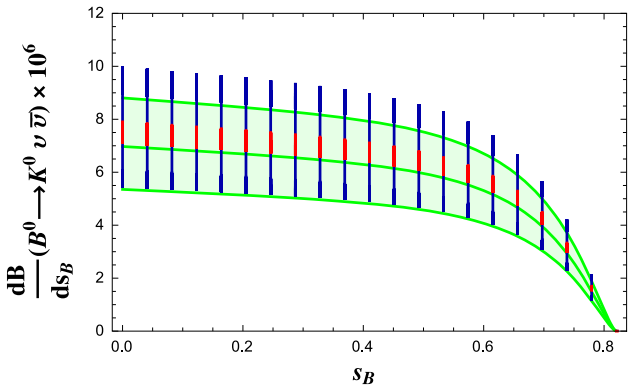

Fig. 3 $\frac{\mathrm{d}\mathscr{B}}{\mathrm{d}s_B}(B^0 \to K^0\nu\bar{\nu})$ distribution in the SM, including the uncertainty on the form factor $F_1(0)$ (*green region*), and in RS$_c$ for the central value of $F_1(0)$ (*red points*) and including the uncertainty of the form factor at $s_B = 0$ (*blue bars*)

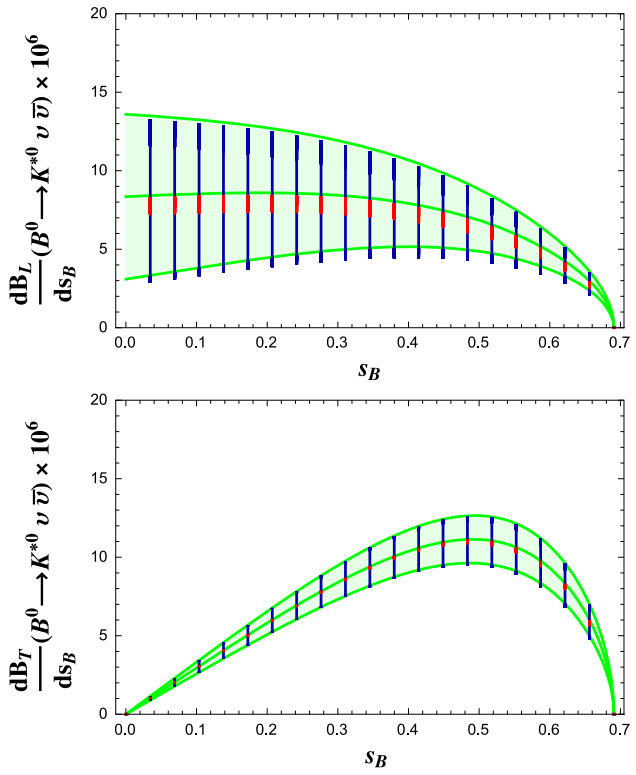

Fig. 4 Distributions $\frac{\mathrm{d}\mathscr{B}_L}{\mathrm{d}s_B}(B^0 \to K^{*0}\nu\bar{\nu})$ (*top*) and $\frac{\mathrm{d}\mathscr{B}_T}{\mathrm{d}s_B}(B^0 \to K^{*0}\nu\bar{\nu})$ (*bottom*). *The green region* corresponds to SM including the uncertainties on the form factors $A_1(0)$, $A_2(0)$ (*top*) and $A_1(0)$, $V(0)$ (*bottom*). *The red dots* and *the blue bars* correspond to RS$_c$, for the central value of the form factors and including their uncertainty at $s_B = 0$, respectively

has a larger uncertainty than the one in (1), due to our more conservative errors on the form factors. The modifications in RS$_c$, obtained for the central value of $F_1(0)$ and accounting for the uncertainty on $F_1(0)$, are also shown in Fig. 3 and produce a prediction for the branching fraction spanning a somewhat wider range,

$$\mathscr{B}(B^0 \to K^0\nu\bar{\nu})_{\mathrm{RS}} \in [3.45 - 6.65] \times 10^{-6}. \tag{48}$$

A similar result is obtained for the charged mode. Hence, the present experimental upper bounds require an improvement by a factor of 3–4 in the case of BaBar, Eq. (3), and of about one order of magnitude in the case of Belle, Eq. (2), to become sensitive to these processes, a task within the possibilities of high-luminosity facilities such as Belle II.

For $B \to K^*\nu\bar{\nu}$ we separately consider the longitudinally and transversely polarized K^*, with distributions in Fig. 4. In RS$_c$ a small deviation from SM is found in the longitudinal distribution. The SM prediction, obtained including the errors on the form factors in quadrature,

$$\mathscr{B}(B^0 \to K^{*0}\nu\bar{\nu})_{\mathrm{SM}} = (10.0 \pm 2.7) \times 10^{-6} \tag{49}$$

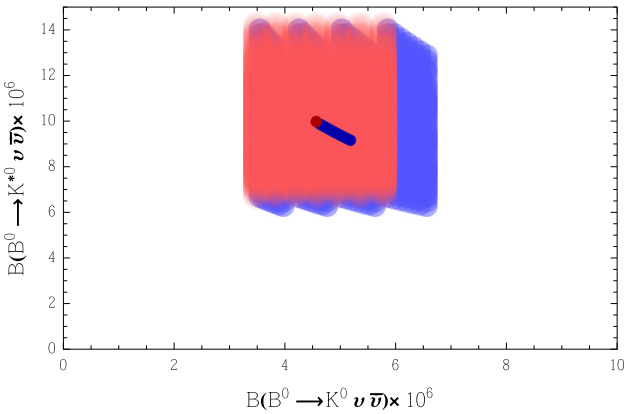

Fig. 5 Correlation between $\mathscr{B}(B^0 \to K^0\nu\bar{\nu})$ and $\mathscr{B}(B^0 \to K^{*0}\nu\bar{\nu})$ obtained varying the RS_c parameters and including the uncertainty on the form factors at $s_B = 0$ (*lighter blue region*). The SM prediction corresponds to the *lighter red region*. *The darker blue curve* and *the darker red dot* correspond to the RS_c and SM prediction, respectively, obtained for the central value of the form factors at $s_B = 0$

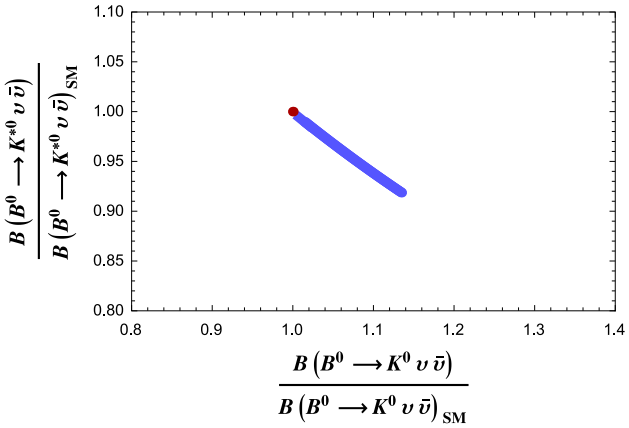

Fig. 6 Correlation between $\mathscr{B}(B^0 \to K^0\nu\bar{\nu})$ and $\mathscr{B}(B^0 \to K^{*0}\nu\bar{\nu})$ (*blue curve*) normalized to the corresponding SM values (*red dot*) obtained for the central value of the form factors

becomes in RS_c the range

$$\mathscr{B}(B^0 \to K^{*0}\nu\bar{\nu})_{\mathrm{RS}} \in [6.1 - 14.3] \times 10^{-6}. \tag{50}$$

For the charged mode the predictions are similar. Hence, the required improvement of the current upper bound to reach the expected signal is about a factor of 4 in the case of the Belle upper bounds (2), and about one order of magnitude in the case of the BaBar bounds (3), within the reach of new facilities. Also in the case of K^* our result has a more conservative error than the one quoted in (1). The difference is due to the choice in [7] of exploiting additional information on the measured radiative $B \to K^*\gamma$ decay rate, which results in a reduction of the central value and of the error of the form factors.

Differently from the mode into the pseudoscalar K, the K^* channel allows one to access other observables as the polarization fractions $F_{L,T}$ in (19). Moreover, the measurements of both the K and the K^* modes permit the construction of the fraction R_{K/K^*} in (21), and to study the correlations among the various observables predicted in the SM and in RS_c. Such correlations are important to disentangle different NP scenarios from the one we are investigating. In Fig. 5 we show the correlation between the rates of $B \to K\nu\bar{\nu}$ and $B \to K^*\nu\bar{\nu}$, with the inclusion of the hadronic uncertainty. Although the effects of the form factor errors are at present noticeable, the SM and the RS_c predictions already have a non-overlapping region, which is interesting in view of the envisaged possibility of reducing the hadronic uncertainty. In particular, the K and K^* modes are anticorrelated, hence a reduction of the $B \to K^*\nu\bar{\nu}$ decay rate goes in RS_c with an increase of the rate of $B \to K\nu\bar{\nu}$ with respect to the SM, as is visible in Fig. 6 in the ideal case of an exact knowledge of the hadronic matrix elements.

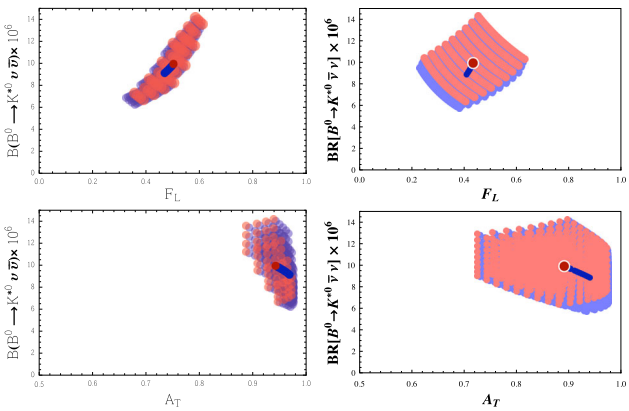

Fig. 7 $\mathscr{B}(B^0 \to K^{*0}\nu\bar{\nu})$ versus $F_L(B^0 \to K^{*0}\nu\bar{\nu})$ (*top*) and $A_T(B^0 \to K^{*0}\nu\bar{\nu})$ (*bottom*), varying the RS_c parameters in the allowed ranges and including the uncertainty on the form factors at $s_B = 0$ (*lighter blue regions*) from LCSR (*left*) and from lattice QCD [53] (*right*). The SM predictions correspond to the *lighter red regions*. *The darker blue curves* and *the darker red dots* correspond to the RS_c and SM predictions, respectively, for the central value of the form factors

As for the longitudinal K^* polarization fraction, the differential distribution in Fig. 8 has a small deviation and can be below the SM; the correlation of the integrated fraction with the branching rate is depicted in Fig. 7. A precise correlation pattern hence exists in RS_c among the three observables $\mathscr{B}(B \to K\nu\bar{\nu})$, $\mathscr{B}(B \to K^*\nu\bar{\nu})$, and F_L: the first one can be above, the other one below its SM values. We also show illustratively the correlation between the transverse asymmetry A_T in (22) in $B \to K^*\nu\bar{\nu}$ and the branching fraction in the SM and RS_c, Fig. 7, for which the two models, with the present hadronic uncertainty, have a big overlap.

The observable R_{K/K^*} defined in Eq. (21) and obtained from the K and K^* measurements is depicted in Fig. 9 versus F_L. A sizable form factor uncertainty is still present, at odds with the expectation that such a variable should be quite safe; nevertheless, a region where SM and RS_c results do not over-

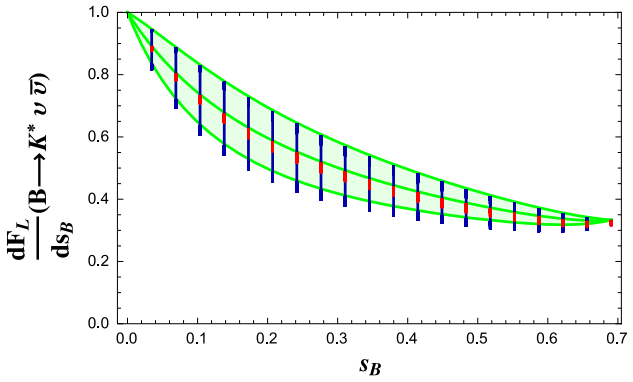

Fig. 8 Differential longitudinal K^* polarization fraction $\frac{dF_L}{ds_B}(B^0 \to K^{*0}\nu\bar{\nu})$ in the SM including the uncertainties on $A_1(0)$, $A_2(0)$, and $V(0)$ (*green region*), and in RS_c for the central values of $A_1(0)$, $A_2(0)$ and $V(0)$ (*red points*) and with the error on the form factors (*blue bars*)

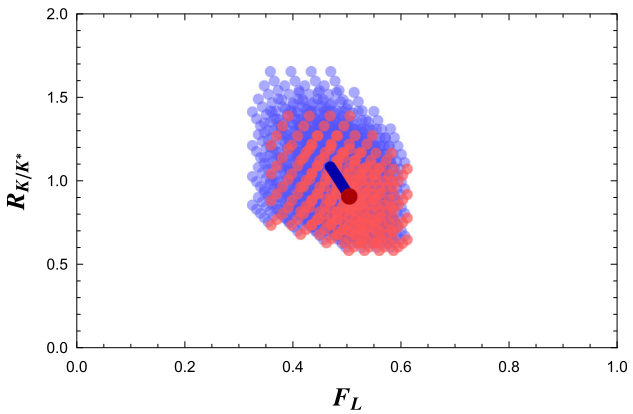

Fig. 9 R_{K/K^*}, defined in Eq. (21), versus $F_L(B^0 \to K^{*0}\nu\bar{\nu})$. The *color code* is the same as in Fig. 7

lap can be observed, together with the anticorrelation with F_L.

An important issue concerns the hadronic error, the reliability of which cannot be asserted without the comparison among form factors obtained by independent nonperturbative methods. Recent lattice QCD determinations of the $B \to K^{(*)}$ form factors [52,53] can be used to estimate the size of the hadronic uncertainties affecting the various observables we have considered. Using the set in [53] we have analyzed, e.g., the correlation among the $B \to K^*\nu\bar{\nu}$ decay rate and F_L and A_T. The results reported in Fig. 7 show that the predictions already obtained are robust within the quoted errors.

7 Role of the right-handed operators in RS_c

The correlation between ε and η is of particular interest, in the light of general analyses where the effects of Z' neutral gauge bosons are considered with no reference to the underlying NP theory [18]. In such analyses, several possible non-diagonal couplings to left- and right-handed quarks lead to models that can be distinguished by the relative weight of the couplings. As an example, a left-right symmetric scenario (LRS) corresponds to Z' left- and right-handed couplings equal in size and sign; the $\varepsilon - \eta$ correlation is different in the various cases.

Comparing our result in Fig. 2 with the various possibilities considered in the general analysis, Fig. 20 of [18], we infer that the RS_c model looks similar to the RHS scenario, with a Z' mainly coupled to right-handed quarks. Indeed, the difference $C_L^{RS} - C_L^{SM}$ and the coefficient C_R^{RS}, playing the role of the left- and right-handed quark couplings to a new gauge boson, have opposite sign, and $C_R^{RS} \gg C_L^{RS} - C_L^{SM}$, Fig. 1. Although in RS_c there are several additional gauge boson, the effect is similar to the case of one new boson.

The correlation of $\mathcal{B}(B \to K\nu\bar{\nu})$ and $\mathcal{B}(B \to K^*\nu\bar{\nu})$ with $\mathcal{B}(B_s \to \mu^+\mu^-)$ provides a deeper insight. In NP models one has

$$\frac{\mathcal{B}(B_s \to \mu^+\mu^-)}{\mathcal{B}(B_s \to \mu^+\mu^-)|_{SM}} = \frac{C_{10} - C'_{10}}{C_{10}^{SM}} \tag{51}$$

where C_{10} and C'_{10} are the Wilson coefficients of the semileptonic electroweak penguin operators with axial vector leptonic current and $V - A$ and $V + A$ structure of the quark current in the effective $b \to s\ell^+\ell^-$ Hamiltonian. In SM only C_{10}^{SM} is relevant (the contribution of O'_{10} is negligible). Evaluating $C_{L,R}$, C_{10}, and C'_{10} in the RS_c parameter space, the correlations in Fig. 10 are found. The rates of $B \to K\nu\bar{\nu}$ and $B_s \to \mu^+\mu^-$ are anticorrelated: in RS_c a larger $\mathcal{B}(B_s \to \mu^+\mu^-)$ than in the SM implies a lower $\mathcal{B}(B \to K\nu\bar{\nu})$. The opposite happens for $B \to K^*\nu\bar{\nu}$: $\mathcal{B}(B \to K^*\nu\bar{\nu})$ and $\mathcal{B}(B_s \to \mu^+\mu^-)$ are correlated, therefore finding one of them above its SM value would require an enhancement also of the other one. This again characterizes RS_c as an RHS scenario, as one can infer from a comparison with the general result of Fig. 21 in [18].

8 $B_s \to (\phi, \eta, \eta', f_0(980))\bar{\nu}\nu$ in RS_c

Several B_s decay modes of great phenomenological interest are driven by the transition $b \to s\nu\bar{\nu}$. Here we focus on $B_s \to (\eta, \eta')\nu\bar{\nu}$, on the decay $B_s \to \phi\nu\bar{\nu}$ and on $B_s \to f_0(980)\nu\bar{\nu}$ with the scalar $f_0(980)$ meson in the final state, all of them accessible at the new facilities.

The modes into η and η' must be considered altogether, due to the η–η' mixing. Two schemes are usually adopted to describe this mixing, in either the singlet-octet (SO) or the quark-flavor (QF) basis, and both schemes involve two mixing angles [54–56]. We choose the quark-flavor basis, defining

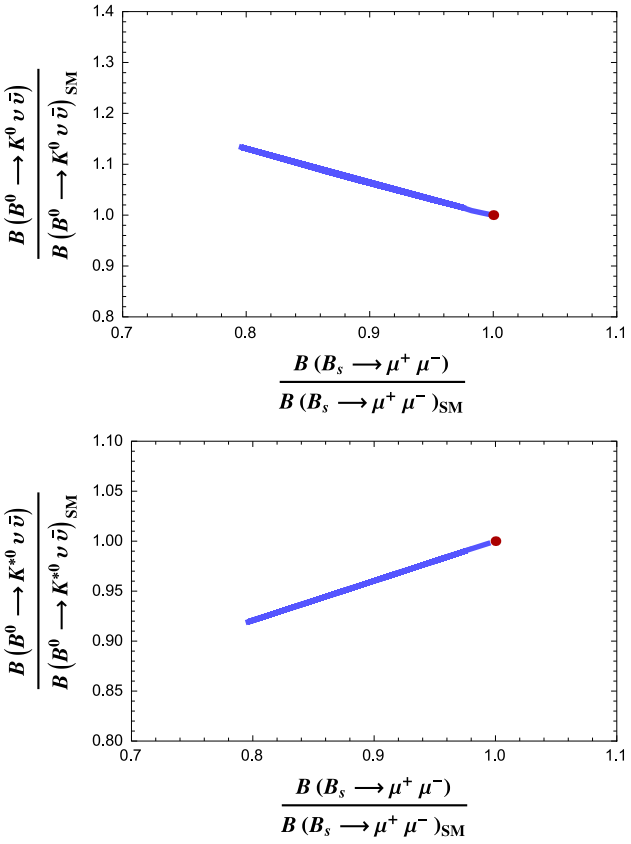

Fig. 10 Correlation between $\mathscr{B}(B^0 \to K^0\nu\bar{\nu})$ and $\mathscr{B}(B_s \to \mu\bar{\mu})$ (*top*), and between $\mathscr{B}(B^0 \to K^{*0}\nu\bar{\nu})$ and $\mathscr{B}(B_s \to \mu\bar{\mu})$ (*bottom*) normalized to their central SM values. The hadronic uncertainty is not included. *The blue lines* correspond to RS_c, *the red dots* to the SM

$$|\eta_q\rangle = \frac{1}{\sqrt{2}}\left(|\bar{u}u\rangle + |\bar{d}d\rangle\right),$$
$$|\eta_s\rangle = |\bar{s}s\rangle, \tag{52}$$

in which the two mixing angles φ_q and φ_s,

$$|\eta\rangle = \cos\varphi_q\,|\eta_q\rangle - \sin\varphi_s\,|\eta_s\rangle,$$
$$|\eta'\rangle = \sin\varphi_q\,|\eta_q\rangle + \cos\varphi_s\,|\eta_s\rangle, \tag{53}$$

differ by OZI-violating effects. However, the difference is experimentally found to be small ($\varphi_q - \varphi_s < 5^\circ$); therefore, within the present accuracy we can adopt an η–η' mixing description in the QF basis and a single mixing angle $\varphi_q \simeq \varphi_s \simeq \varphi$. This choice is supported by a study of the radiative $\phi \to \eta\gamma$ and $\phi \to \eta'\gamma$ transitions [57]. The KLOE Collaboration has measured the ratio $\dfrac{\Gamma(\phi \to \eta'\gamma)}{\Gamma(\phi \to \eta\gamma)}$, finding for the η–η' mixing angle the value $\varphi = \left(41.5 \pm 0.3_{\mathrm{stat}} \pm 0.7_{\mathrm{syst}} \pm 0.6_{th}\right)^\circ$ [58]. An improved analysis by the same collaboration, allowing a gluonium content in the η' and making use of the measured ratio $\frac{\Gamma(\eta' \to \gamma\gamma)}{\Gamma(\pi^0 \to \gamma\gamma)}$ confirms this determination of φ [59].

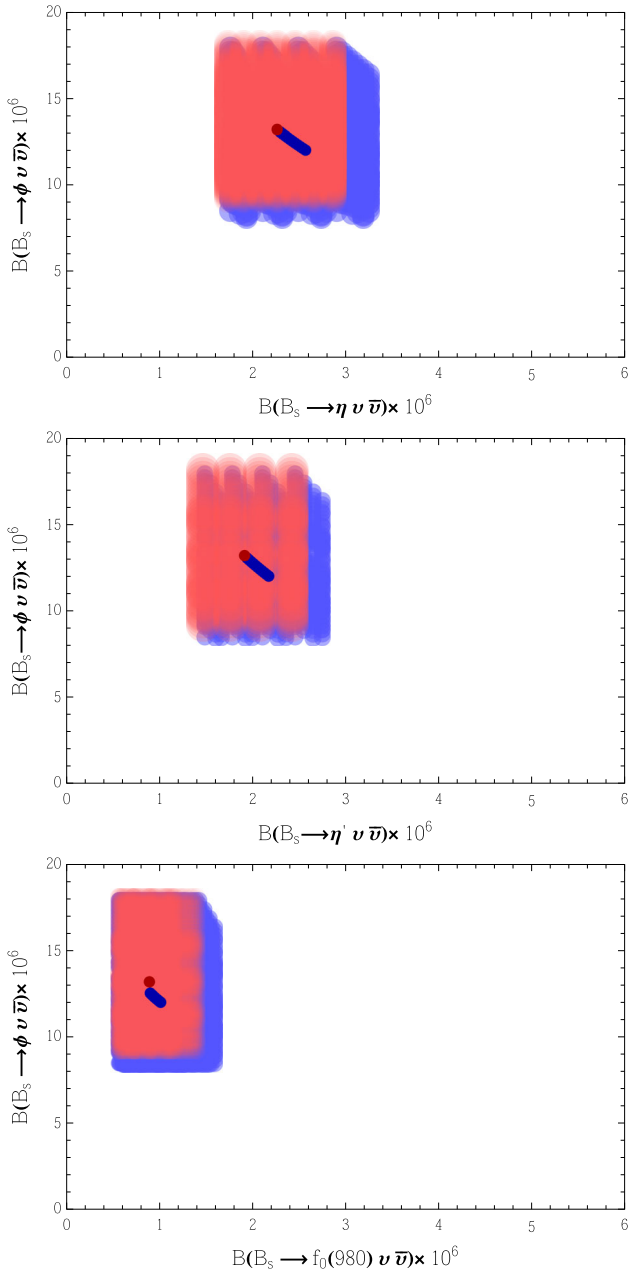

Fig. 11 Correlation of $\mathscr{B}(B_s \to \phi\nu\bar{\nu})$ with $\mathscr{B}(B_s \to \eta\nu\bar{\nu})$ (*top*), $\mathscr{B}(B_s \to \eta'\nu\bar{\nu})$ (*center*) and $\mathscr{B}(B_s \to f_0(980)\nu\bar{\nu})$ (*bottom*). The *color code* is the same as in Fig. 7

The flavor symmetry permits to relate the $B_s \to \eta, \eta'$ form factors to the $B \to K$ ones. For a form factor F one has $F^{B_s\to\eta} = -\sin\varphi F^{B\to K}$ and $F^{B_s\to\eta'} = \cos\varphi F^{B\to K}$ [60]. On the other hand, for the $B_s \to \phi\nu\bar{\nu}$ mode we use the LCSR $B_s \to \phi$ form factors in Refs. [49,50].

The SM predictions, obtained for $\tau(B_s) = 1.512 \pm 0.007$ ps [14],

$$\mathscr{B}(B_s \to \eta\nu\bar{\nu})_{\mathrm{SM}} = (2.3 \pm 0.5) \times 10^{-6}, \tag{54}$$
$$\mathscr{B}(B_s \to \eta'\nu\bar{\nu})_{\mathrm{SM}} = (1.9 \pm 0.5) \times 10^{-6}, \tag{55}$$

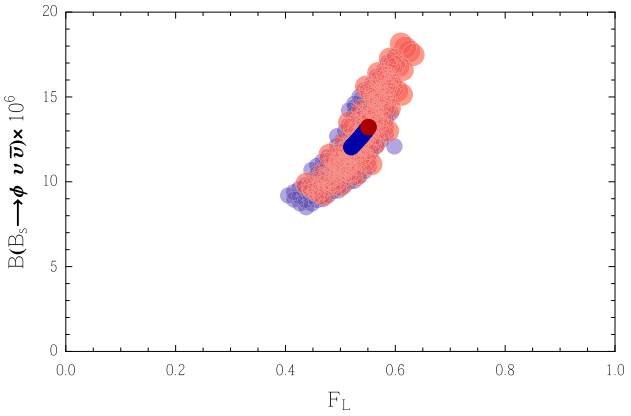

Fig. 12 $\mathscr{B}(B_s \to \phi\nu\bar{\nu})$ versus $F_L(B_s \to \phi\nu\bar{\nu})$. The *color code* is the same as in Fig. 7

$$\mathscr{B}(B_s \to \phi\nu\bar{\nu})_{\rm SM} = (13.2 \pm 3.3) \times 10^{-6} \tag{56}$$

are modified in RS$_c$:

$$\mathscr{B}(B_s \to \eta\nu\bar{\nu})_{\rm RS} \in [1.7 - 3.3] \times 10^{-6}, \tag{57}$$
$$\mathscr{B}(B_s \to \eta'\nu\bar{\nu})_{\rm RS} \in [1.5 - 2.8] \times 10^{-6}, \tag{58}$$
$$\mathscr{B}(B_s \to \phi\nu\bar{\nu})_{\rm RS} \in [8.4 - 18.0] \times 10^{-6}. \tag{59}$$

The result is particularly relevant in the case of the $B_s \to \phi$ mode, which should be the first one accessible for the B_s meson: the rate is within the reach of the new facilities, the ϕ can easily be identified and its decay modes allow one to construct, e.g., the F_L observable. The various correlation patterns are shown in Fig. 11: anticorrelation is found between the rates of $B_s \to \eta^{(\prime)}\nu\bar{\nu}$ with $B_s \to \phi\nu\bar{\nu}$. For F_L the results are depicted in Fig. 12.

The last mode in our analysis involves the scalar $f_0(980)$ meson. The $B_s \to f_0(980)$ form factors have been determined assuming for $f_0(980)$ a dominant quark–antiquark $s\bar{s}$ structure [61]. With the updated value of $\tau(B_s)$ we find that the SM prediction is modified in RS$_c$:

$$\mathscr{B}(B_s \to f_0(980)\nu\bar{\nu})_{\rm SM} = (8.95 \pm^{2.9}_{2.5}) \times 10^{-7}, \tag{60}$$
$$\mathscr{B}(B_s \to f_0(980)\nu\bar{\nu})_{\rm RS} \in [5 - 17] \times 10^{-7}. \tag{61}$$

This channel should be accessible through the $f_0(980) \to \pi\pi$ transition, providing another test of the RS$_c$ scenario.

9 Conclusions

Although experimentally challenging, the FCNC exclusive b-hadron transitions into $\nu\bar{\nu}$ pairs are of great interest, as they can provide the evidence of possible deviations from SM through signals of remarkable theoretical significance. We have examined a set of B and B_s decay modes in the RS$_c$ model, with emphasis on the correlations among the observables that are features of the model. In the planned experimental analyses these modes can be accessible, and the predictions presented here will become testable.

References

1. G. Isidori, Y. Nir, G. Perez, Ann. Rev. Nucl. Part. Sci. **60**, 355 (2010). arXiv:1002.0900 [hep-ph]
2. A.J. Buras, J. Girrbach, Rep. Prog. Phys. **77**, 086201 (2014). arXiv:1306.3775 [hep-ph]
3. G. Isidori, F. Teubert, Eur. Phys. J. Plus **129**, 40 (2014). arXiv:1402.2844 [hep-ph]
4. A.J. Buras, arXiv:hep-ph/9806471
5. P. Colangelo, F. De Fazio, P. Santorelli, E. Scrimieri, Phys. Lett. B **395**, 339 (1997). arXiv:hep-ph/9610297
6. D. Melikhov, N. Nikitin, S. Simula, Phys. Lett. B **428**, 171 (1998). arXiv:hep-ph/9803269
7. W. Altmannshofer, P. Ball, A. Bharucha, A.J. Buras, D.M. Straub, M. Wick, JHEP **0901**, 019 (2009). arXiv:0811.1214 [hep-ph]
8. W. Altmannshofer, A.J. Buras, D.M. Straub, M. Wick, JHEP **0904**, 022 (2009). arXiv:0902.0160 [hep-ph]
9. A.J. Buras, J. Girrbach-Noe, C. Niehoff, D.M. Straub, JHEP **1502**, 184 (2015). arXiv:1409.4557 [hep-ph]
10. O. Lutz et al. (Belle Collaboration), Phys. Rev. D **87**(11), 111103 (2013). arXiv:1303.3719 [hep-ex]
11. J.P. Lees et al. (BaBar Collaboration), Phys. Rev. D **87**(11), 112005 (2013). arXiv:1303.7465 [hep-ex]
12. P. del Amo Sanchez et al. (BaBar Collaboration), Phys. Rev. D **82**, 112002 (2010). arXiv:1009.1529 [hep-ex]
13. J. Beringer et al. (Particle Data Group Collaboration), Phys. Rev. D **86**, 010001 (2012)
14. Y. Amhis et al. (Heavy Flavor Averaging Group Collaboration), arXiv:1207.1158 [hep-ph]. http://www.slac.stanford.edu/xorg/hfag/
15. C.S. Kim, Y.G. Kim, T. Morozumi, Phys. Rev. D **60**, 094007 (1999). arXiv:hep-ph/9905528
16. G. Buchalla, G. Hiller, G. Isidori, Phys. Rev. D **63**, 014015 (2000). arXiv:hep-ph/0006136
17. D.M. Straub, JHEP **1308**, 108 (2013). arXiv:1302.4651 [hep-ph]
18. A.J. Buras, F. De Fazio, J. Girrbach, JHEP **1302**, 116 (2013). arXiv:1211.1896 [hep-ph]
19. P. Colangelo, F. De Fazio, R. Ferrandes, T.N. Pham, Phys. Rev. D **73**, 115006 (2006). arXiv:hep-ph/0604029
20. L. Randall, R. Sundrum, Phys. Rev. Lett. **83**, 3370 (1999). arXiv:hep-ph/9905221
21. K. Agashe, R. Contino, L. Da Rold, A. Pomarol, Phys. Lett. B **641**, 62 (2006). arXiv:hep-ph/0605341
22. M.S. Carena, E. Ponton, J. Santiago, C.E.M. Wagner, Nucl. Phys. B **759**, 202 (2006). arXiv:hep-ph/0607106
23. G. Cacciapaglia, C. Csaki, G. Marandella, J. Terning, Phys. Rev. D **75**, 015003 (2007). arXiv:hep-ph/0607146
24. M. Blanke, A.J. Buras, B. Duling, K. Gemmler, S. Gori, JHEP **0903**, 108 (2009). arXiv:0812.3803 [hep-ph]
25. P. Biancofiore, P. Colangelo, F. De Fazio, Phys. Rev. D **89**, 095018 (2014). arXiv:1403.2944 [hep-ph]
26. T. Inami, C.S. Lim, Prog. Theor. Phys. **65**, 297 (1981) [Erratum-ibid. **65**, 1772 (1981)]

27. G. Buchalla, A.J. Buras, Nucl. Phys. B **548**, 309 (1999). arXiv:hep-ph/9901288
28. A.F. Falk, M.E. Luke, M.J. Savage, Phys. Rev. D **53**, 6316 (1996). arXiv:hep-ph/9511454
29. U. Egede, T. Hurth, J. Matias, M. Ramon, W. Reece, JHEP **0811**, 032 (2008). arXiv:0807.2589 [hep-ph]
30. M.E. Albrecht, M. Blanke, A.J. Buras, B. Duling, K. Gemmler, JHEP **0909**, 064 (2009). arXiv:0903.2415 [hep-ph]
31. M. Blanke, A.J. Buras, B. Duling, S. Gori, A. Weiler, JHEP **0903**, 001 (2009). arXiv:0809.1073 [hep-ph]
32. A.J. Buras, B. Duling, S. Gori, JHEP **0909**, 076 (2009). arXiv:0905.2318 [hep-ph]
33. M. Blanke, B. Shakya, P. Tanedo, Y. Tsai, JHEP **1208**, 038 (2012). arXiv:1203.6650 [hep-ph]
34. T. Gherghetta, A. Pomarol, Nucl. Phys. B **586**, 141 (2000). arXiv:hep-ph/0003129
35. Y. Grossman, M. Neubert, Phys. Lett. B **474**, 361 (2000). arXiv:hep-ph/9912408
36. B. Duling, PhD thesis: "The custodially protected Randall-Sundrum model: Global features and distinct flavor signatures". Technical University Munich (2010)
37. S. Casagrande, F. Goertz, U. Haisch, M. Neubert, T. Pfoh, JHEP **0810**, 094 (2008). arXiv:0807.4937 [hep-ph]
38. M. Bauer, S. Casagrande, U. Haisch, M. Neubert, JHEP **1009**, 017 (2010). arXiv:0912.1625 [hep-ph]
39. S. Schael et al. (ALEPH and DELPHI and L3 and OPAL and SLD and LEP Electroweak Working Group and SLD Electroweak Group and SLD Heavy Flavour Group Collaborations), Phys. Rep. **427**, 257 (2006). arXiv:hep-ex/0509008
40. G. Burdman, Phys. Rev. D **66**, 076003 (2002). arXiv:hep-ph/0205329
41. G. Burdman, Phys. Lett. B **590**, 86 (2004). arXiv:hep-ph/0310144
42. K. Agashe, G. Perez, A. Soni, Phys. Rev. D **71**, 016002 (2005). arXiv:hep-ph/0408134
43. A.L. Fitzpatrick, G. Perez, L. Randall, Phys. Rev. Lett. **100**, 171604 (2008). arXiv:0710.1869 [hep-ph]
44. S.J. Huber, Q. Shafi, Phys. Lett. B **498**, 256 (2001). arXiv:hep-ph/0010195
45. S.J. Huber, Nucl. Phys. B **666**, 269 (2003). arXiv:hep-ph/0303183
46. K. Agashe, G. Perez, A. Soni, Phys. Rev. Lett. **93**, 201804 (2004). arXiv:hep-ph/0406101
47. P.R. Archer, S.J. Huber, S. Jager, JHEP **1112**, 101 (2011). arXiv:1108.1433 [hep-ph]
48. J.P. Lees et al. (BaBar Collaboration), Phys. Rev. D **86**, 032012 (2012). arXiv:1204.3933 [hep-ph]
49. P. Ball, R. Zwicky, Phys. Rev. D **71**, 014015 (2005). arXiv:hep-ph/0406232
50. P. Ball, R. Zwicky, Phys. Rev. D **71**, 014029 (2005). arXiv:hep-ph/0412079
51. P. Colangelo, F. De Fazio, P. Santorelli, E. Scrimieri, Phys. Rev. D **53**, 3672 (1996). arXiv:hep-ph/9510403 [Erratum-ibid. D **57**, 3186 (1998)]
52. C. Bouchard et al. (HPQCD Collaboration), Phys. Rev. D **88**(5), 054509 (2013). arXiv:1306.2384 [hep-lat] [Erratum-ibid. D **88**(7), 079901 (2013)]
53. R.R. Horgan, Z. Liu, S. Meinel, M. Wingate, Phys. Rev. D **89**, 094501 (2014). arXiv:1310.3722 [hep-lat]
54. T. Feldmann, P. Kroll, B. Stech, Phys. Rev. D **58**, 114006 (1998). arXiv:hep-ph/9802409
55. T. Feldmann, P. Kroll, B. Stech, Phys. Lett. B **449**, 339 (1999). arXiv:hep-ph/9812269
56. T. Feldmann, Int. J. Mod. Phys. A **15**, 159 (2000). arXiv:hep-ph/9907491
57. F. De Fazio, M.R. Pennington, JHEP **0007**, 051 (2000). arXiv:hep-ph/0006007
58. F. Ambrosino et al. (KLOE Collaboration), Phys. Lett. B **648**, 267 (2007). arXiv:hep-ex/0612029
59. F. Ambrosino et al., JHEP **0907**, 105 (2009). arXiv:0906.3819 [hep-ph]
60. A discussion of this assumption can be found in M.V. Carlucci, P. Colangelo, F. De Fazio, Phys. Rev. D **80**, 055023 (2009). arXiv:0907.2160 [hep-ph]
61. P. Colangelo, F. De Fazio, W. Wang, Phys. Rev. D **81**, 074001 (2010). arXiv:1002.2880 [hep-ph]